2023 IEEE International Conference on Robotics and Automation (ICRA 2023)
May 29 - June 2, 2023. London, UK

Bioinspired tearing manipulation with a robotic fish

Stanley J. Wang[1], Juan Romero[1], Monica S. Li[1], Peter C. Wainwright[2], and Hannah S. Stuart[1*]

***Abstract*— We present SunBot, a robotic system for the study and implementation of fish-inspired tearing manipulations. Various fish species–such as the sunburst butterflyfish–feed on prey fixed to substrates, a maneuver previously not demonstrated by robotic fish which typically specialize for open water swimming and surveillance. Biological studies indicate that a dynamic "head flick" behavior may play a role in tearing off soft prey during such feeding. In this work, we study whether the robotic tail is an effective means to generate such head motions for ungrounded tearing manipulations in water. We describe the function of SunBot and compare the forces that it applies to a fixed prey in the lab while varying tail speeds and ranges of motion. A simplified dynamic template model for the tail-driven head flick maneuver matches peak force magnitudes from experiments, indicating that inertial effects of the fish's body play a substantial role. Finally, we demonstrate a tearing scenario and evaluate a free-swimming trial of SunBot – this is important to show that the actuator that enables swimming also provides the new dual purpose of forceful tearing manipulation.**

I. Introduction

Marine robotic systems can provide sampling services to monitor the health of ocean ecosystems [1], [2], such as living coral reefs on decline [3]. Large conventional marine manipulation systems, e.g. [4], [5], typically require either tethered operation, other vessels and infrastructure, or human oversight. In addition, they can disturb wildlife or damage surroundings [6]. Although new work is emerging to enable soft and effective underwater limbs, grippers and manipulators [7], [8], dexterous manipulation remains an ongoing challenge.

On the other hand, various fish robots have been developed that can monitor the marine environment without disturbing the surroundings [9]. In fact, numerous fish robots have been designed, e.g., [10]–[15], and are smaller than conventional marine robots. These systems are typically intended to perform surveillance or water measurements without contacting the local terrain, and analysis focuses on locomotor ability. In the present work, we explore the possibility of deploying fish robots to perform substrate sampling tasks as well.

A. Fish feeding mechanics

A variety of fish have the ability to bite, scrape or tear prey off of stationary substrates, e.g., [16]–[18]. One interesting feature of some of these fish is a fast lateral body motion called the "head flick" during this type of feeding [19], [20]. The anterior section of the fish moves laterally after biting the prey, to apply forces both normal to and in the plane of the surface. It is hypothesized that this behavior helps to tear the prey free from the substrate, and that the strong locomotor muscles of the fish propel this dynamic maneuver. This is important because, if true, it means that the actuators used to articulate robotic fish tail-fins could serve dual purposes – for both locomotion and tearing forces for sample collection.

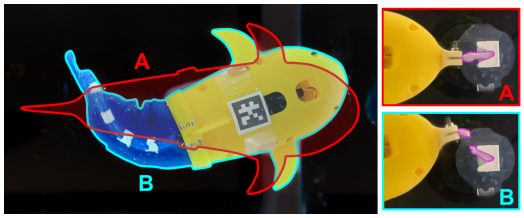

Fig. 1. SunBot is capable of exerting forces useful in floating manipulation through a rapid tail motion. (a) Red outlines denote the initial fish pose, with the head attached to an affixed paper 'specimen.' (b) Cyan outlines denote the tearing of the paper through a rapid tail-driven head flick. The 'specimen' is outlined in magenta in both (a) and (b).

Substrate-feeding fish possess intricate jaw structures [19], [21]. Such specialized jaws provide features for the biting of prey from a variety of surfaces, securing it between the jaws before performing the head flick [20]. In the present work, we look only at the role of the tail fin in floating-body manipulation dynamics, and leave the study and implementation of a robotic jaw gripper to future work.

B. Manipulation with a floating platform

In the current work we assume that the fish is a neutrally buoyant floating body. Therefore, the force it can apply to a surface will be limited largely by the inertial and fluid forces generated by motion of the body and fins in water. A significant set of literature has been developed around the dynamics of dexterous manipulation with floating bodies in underwater, aerial and space applications [22]–[24], but these do not consider the explicit use of fish-inspired strategies.

In prior robotics work with marine remotely operated vehicles (ROV), it has been suggested to anchor the vehicle to the substrate in order to facilitate fine manipulations, by avoiding the floating manipulation task altogether [25]. In another work, the ROV sets down on the ocean floor when applying tugging forces and uses scissors to cut at soft corals [26]. Other floating manipulators use large thrusters and massive machinery, on the order of 100 kg to provide contact forces [4]. The present work studies floating-body force application using the fish-inspired head flick method for small-scale robots, on the order of < 1 kg.

[1] Authors are with the Dept. of Mechanical Engineering, University of California Berkeley, Berkeley, CA, USA.
[2] Author is with the Dept. of Evolution and Ecology, University of California Davis, Davis, CA, USA.
* Corresponding author (email: hstuart@berkeley.edu)
This paper has a supplemental video associated with it.

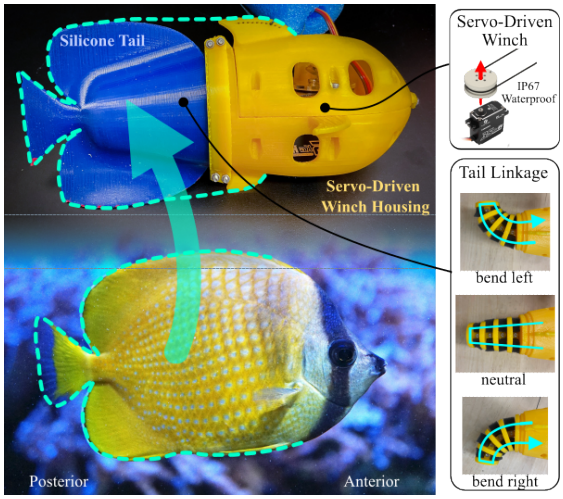

Fig. 2. SunBot (top) is inspired by the sunburst butterflyfish (bottom), which exhibits lateral head motions when tearing prey away from substrates. Primary features include a servo-driven winch housed in a rigid plastic shell, and cable-actuated tail linkage encased in a silicone tail. Photo credit (*C. kleinii* only): Tiia Monto, CC BY-SA 4.0 via Wikimedia Commons.

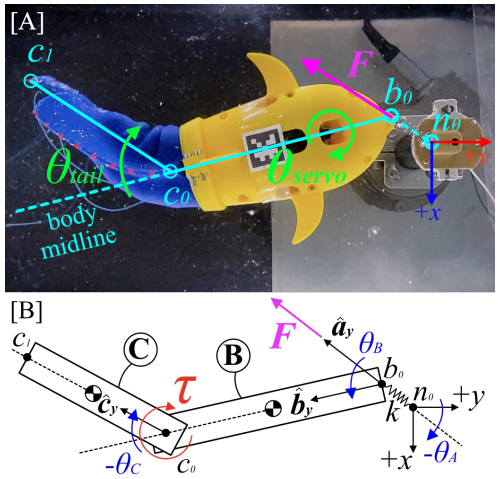

Fig. 3. (a) The reference frame, key geometric points, and actuation and tail angles used to describe fish behavior F is the applied force by the fish to the end of the prey. (b) The corresponding parameters and variables used for the template model of the tail-driven maneuver, including the torque applied between bodies B and C, τ.

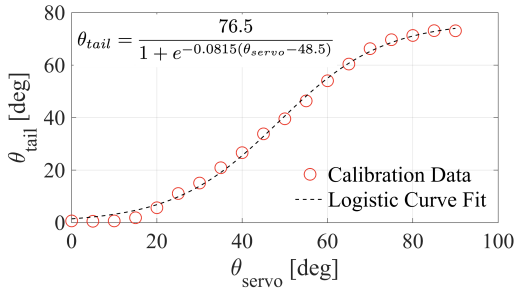

Fig. 4. The relationship between internal servomotor command angle and observed tail angle can be modeled by a logistic function.

C. Overview

We present SunBot (Sunburst Robot), a robotic fish that can impart forces at its head by flicking its tail–a behavior inspired by similar feeding action observed in sunburst butterflyfish (*Chaetodon kleinii*). To the authors' knowledge, this is the first application of robotic tail actuation for tearing soft material off of a fixed substrate, as demonstrated in Fig. 1. Section II describes the implementation of the robophysical model. Section III describes the laboratory setup and tests used to study the role of tail actuation on the forces applied to both mock and real prey, with results reported in Section IV. A simplified two-body dynamic simulation (defined in Section II) matches with force trends, informing our understanding of this maneuver in the robotic system. We discuss the results of laboratory experiments in Section V, and demonstrate more realistic tearing and swimming abilities of SunBot in Section VI. We conclude in Section VII that our work shows the potential of locomotor actuators in robotic fish to also support ungrounded tearing manipulation, motivating new areas of future work.

II. Robophysical Models

This section first describes the mechanical implementation of SunBot. It then defines a proposed dynamics model to predict the forces imparted by this robot to a compliant prey.

A. Robotic hardware model

We perform experimental study using SunBot which serves as a robophysical model emulating feeding events of browsing corallivores. The foundational component of the robot is a mechanical tail actuator designed with capabilities for both rapid dynamic movements as well as sustained Body-Caudal Fin (BCF) swimming locomotion [27]. This is achieved by implementing a cable-driven backbone embedded within a compliant passive tail structure, as in [15], [28]. As shown in Fig. 2, the articulated tail mechanism consists of 5 rigid links coupled with pin joints and controlled by a cable drive. Tension applied to either end of the cable results in an overall lateral deflection of the tail backbone. This mechanism is then encased by a soft tail cast out of a Shore 10A silicone (DragonSkin™10). The particular geometry of the compliant tail contour is modelled after the morphology of the sunburst butterflyfish tail, with enlarged soft dorsal/anal fins and a small caudal fin.

The cable-actuated tail structure is directly driven by a 3.8 cm diameter winch fastened to a high-torque IP67 waterproof servo. (FlashHobby M35CHW). The servo is secured inside the rigid body of the robot, which is 3D-printed with holes to allow for water ingress. The robot is tethered to a small flotation device to ensure it remains in a balanced orientation and consistent depth under water. Power and PWM signal to control the servo are routed through wires to an external power source and motor-driver/microcontroller above water. An open-loop control trajectory is implemented with both the stroke of actuation (θ_{tail}), as defined in Fig. 3(a), as well as the speed of actuation (ω_{tail}) as tuning parameters. We observe that there is a nonlinear correlation between the commanded servo position and realized tail position, which is empirically modeled by a logistic relationship in Fig. 4.

B. Simplified rigid-body model

As shown in Fig. 3 (b), we model the fish as two rigid cuboid bodies, B and C, connected by a frictionless pin joint located at point C_o. The most anterior point of the fish, B_o, is connected to a massless linear spring representing the prey with stiffness k connected to the world reference point N_o with initial length L_o. The tip of the tail is point C_1. We assume that the body is neutrally buoyant and neglect gravity. We also neglect water effects like drag. The spring can both stretch and rotate by angle θ_a while the orientation of body B is defined relative to the orientation of the spring by θ_b. The tail angle, θ_c is the orientation of body C relative to body B. We define $\theta_{tail} = |\theta_c|$. Constant parameters of the model are reported in Table I.

TABLE I
CONSTANT PARAMETERS FOR DYNAMICS MODEL.

Parameter	Description	Value
m_b	Mass of body B	250 g
m_c	Mass of body C	150 g
L_B	Body B length in $\hat{b}_y$	15 cm
L_C	Body C length in $\hat{c}_y$	11 cm
w_B, w_C	B & C widths in $\hat{b}_x/\hat{c}_x$	2 cm
h_B, h_C	B & C heights in $\hat{n}_z$	6 cm
L_o	Neutral spring length	2.4 cm
k	Spring stiffness	4.8 N/cm

A single actuator is modelled to apply torque magnitude, τ, between bodies B and C. The torque is controlled using a feed-forward control law to track a desired tail trajectory $\theta_{c,des} = f(t)$ such that $\ddot{\Delta} + 2\zeta w_n \dot{\Delta} + w_n^2 \Delta = 0$ where $\Delta = \theta_{c,des} - \theta_c$, ζ = 1 and ω_n = 10 rad/sec. We set $\theta_{c,des}$ as a 3rd order polynomial fit between initial and final pose over a duration of time, with zero velocity at start and stop. We match these trajectory input parameters to empirically observed tail motions during experiments for comparison between the dynamics model and the real SunBot behavior. All simulations are performed using MotionGenesis dynamics simulator and MATLAB.

III. EXPERIMENTAL METHODS

A. Experimental setup

Throughout laboratory experiments, we use a 3D force-measurement apparatus designed for collection of synchronous force and video data. As shown in Fig. 5, the main component of the experimental assembly is a 6-axis Force/Torque sensor (ATI Gamma IP65 with SI-32-2.5 calibration) located above the water, with a carbon fiber arm extending down into the water. In force characterization experiments, we emulate a compliant prey using a spring (12.5 mm natural length, 480 N/m stiffness) with two cylindrical neodymium magnets (3 mm length, 8 mm diameter) adhered at the ends. Two spherical neodymium magnets (6.35 mm diameter, 4.44 N max pull force) are each fixed to the anterior tip of SunBot and the end of the force sensitive rod. During relative movements between the fish and pedestal, there is sliding contact between the magnets. The neutral distance from center-to-center of the spherical magnets is 24 mm.

To visualize SunBot while it interacts with prey, we capture video from below the tank at 240 frames per second. An LED is wired to our data acquisition system as a visual marker for synchronization of force and video data. For motion tracking, we affix ArUco markers to the bottom of the tank for world-frame reference and to the ventral side of SunBot's head for pose of the rigid head. We also add red markers approximately 1 cm apart to the soft fin below the robot, as shown in Fig. 3(a). In video post-processing, OpenCV is used to track body orientation over the course of a trial and a color filter is applied to identify the centroid of each of the red dots along the tail for pose tracking.

B. Force characterization

We collect force and video data while varying range of motion and speed. Range of motion (RoM) for θ_{tail} is varied between 17, 37, 60 and 72°. For each range of motion, the servo speed is commanded at 100, 200, 300, 400 °/s; in actuality the speed varies with range of motion resulting in the achieved speeds reported in Table II.

TABLE II
ACHIEVED TAIL SPEEDS ACROSS RANGE OF MOTION (ROM).

	Speed [°/s]			
Command:	100	200	300	400
RoM: 17°	170	350	530	630
RoM: 37°	140	280	460	610
RoM: 60°	130	240	380	480
RoM: 72°	130	270	390	480

Three trials are conducted at each condition, for a total of 48 trials. For each trial, the robot is allowed to float freely while attached to the spring until it reaches a neutral position, with the body-axis aligned roughly along $\hat{y}$. We then command a desired servo actuation speed and a desired servo angle to the robot to bend the body to one side at a particular rate and amplitude, respectively. After data collection, the robot then returns its tail to the neutral position in preparation for the next trial.

Each trial is filtered using a low-pass filter with cutoff frequency of 60 Hz, followed by a 3rd-order Savitzy-Golay

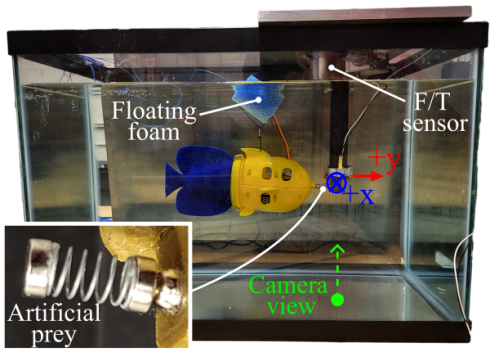

Fig. 5. Side-view of aquarium tank filled with water with force measurement apparatus resting on top. The SunBot platform is attached to the end mount of the force measurement device via artificial prey (lower left) consisting of a spring and magnetic attachment at either end. A camera is used to capture video data from below.

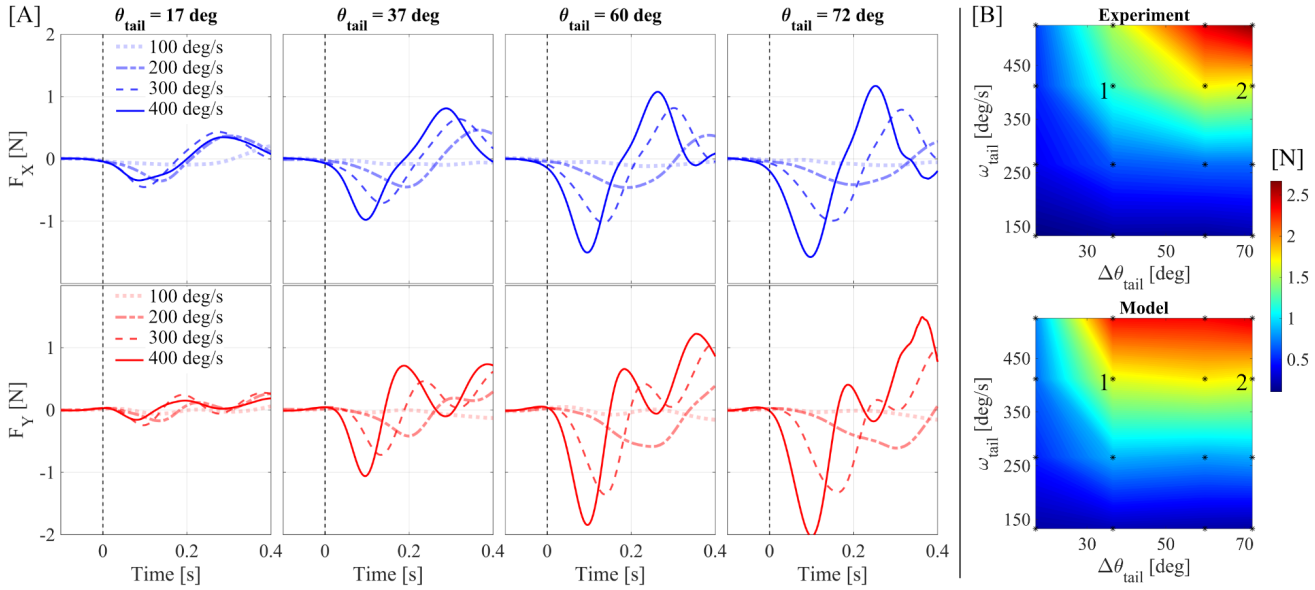

Fig. 6. Head flick forces of SunBot. (a) Measured temporal force profiles in the x and y-directions for commanded angular velocities (100, 200, 300, 400 °/s) and range of motion (17, 37, 60, 72°). The initial negative peak is substantial, and the oscillations afterwards are due to inertial and spring effects. (b) aggregated peak net force magnitude, comparing the experimental measurements to the dynamic rigid-body model.

filter. After filtering, the three trials are averaged to obtain an aggregate representative force profile for each condition.

C. Comparison with sunburst butterflyfish

Analogous force and video data is collected with a single sunburst butterflyfish specimen. The fish is allowed to feed off of a piece of shrimp attached to the same force measurement setup used for robotic trials. The force and motion of a single trial from the real animal is then compared with one produced by the robotic fish. Animal procedures were approved by the UC Davis Animal Care and Use Committee.

IV. Laboratory Results

A. Robotic results

Aggregate force measurement results are plotted in Fig. 6(a) across all test conditions. For all trials, the primary tugging event is applied in the negative $\hat{x}$ lateral direction and the negative $\hat{y}$ axial direction, corresponding to a pulling away from the surface with the spring in tension. When the $\hat{y}$ component of force crosses the zero axis after the initial peak, we see that the spring goes into compression and begins to oscillate. In looking at the initial pulling events, we observe a faster actuation timescale at higher tail speeds with a secondary dependence on tail angle. While subtle, the peak forces in the $\hat{x}$ and $\hat{y}$ directions also occur at different times at smaller actuation speeds, with lateral force in $\hat{x}$ leading the outward component in $\hat{y}$. As actuation speed increases, the lag between peak force occurrence in lateral and axial directions becomes negligible. In subsequent free oscillations after the initial pulling impulse is applied, we observe a slight inverse correlation between oscillation periods and actuation speeds. Furthermore, the subsequent lateral oscillation in $\hat{x}$ is not in phase with that in $\hat{y}$ due to the discrepancy in spring constant along the two directions.

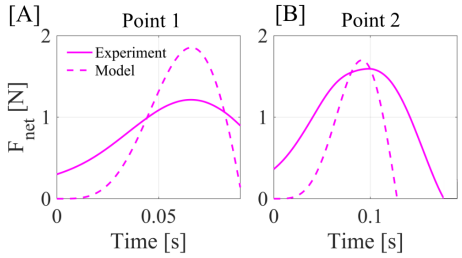

Fig. 7. Comparison plots between measured and simulated net force magnitudes over time for the points labeled (a) '1' and (b) '2' in Fig. 6(b).

The initial pulling peak in tension is recorded and plotted in Fig. 6(b, top). At higher actuation angles, we find a roughly linear relationship between tail speed and force application. At low tail angles, SunBot applies very little force even at higher speeds. The highest force of 2.7 N occurs with the fastest tail angle at the largest range of motion. The smallest force of 0.1 N occurs at the smallest speed and range of motion tested.

The peak force magnitudes resulting from rigid-body simulations conducted across the same set of control parameters as the experiments are shown in Fig. 6(b, bottom). On whole, the simulation appears to capture similar trends and overall force magnitudes as the experiments for the range of parameters tested. However, it appears that the simulation overestimates applied force at low tail angles and underestimates applied force at the highest speed and tail angle condition. Fig. 7 shows the force-time plots for the two cases, labeled '1' and '2' in Fig. 6(b), comparing experimental forces measured with the simulated results. Note that the experimental peak is aligned in time to match the simulation peak. Case 1 is the worst case performance of the simulation, with a large discrepancy in estimated net peak force, while

case 2 demonstrates an outcome with very similar peak amplitudes. In both cases, the dynamics simulation shows the pulling event happening over a shorter duration of time than the timescale observed for the experiments.

In both experiment and simulation, we observe the peak pulling force often occurs prior to the end of the tail actuation motion. This gives rise to a potential saturation in the stroke of the tail actuation, where a further increase in the range of motion provides a negligible improvement in peak pulling force. From Fig. 6(b), we observe that both experimental and simulated results exhibit this saturation to an extent. For empirical data, we see that tail angles of $\theta_{tail} = 60, 72°$ produce a relatively similar peak force for a given angle. A similar saturation can be observed for the simulated results albeit at a lower angle, with $\theta_{tail} = 37, 60, 72°$ all yielding relatively similar peak forces for a given speed.

B. Sunburst butterfly comparison results

The headflick motion for a sunburst butterflyfish specimen, *C. kleinii* is depicted in Fig. 8(a). Fig. 8 also shows a direct visual comparison between trials with a real butterflyfish and SunBot (conditions: 60°, 300°/s). Both cases show a negative peak during pulling and time scales on a similar order of magnitude. The force scales differ by an order or magnitude. The amount of time *C. kleinii* exerted forces on prey in Fig. 8(a) was less than 50 ms, whereas the force on the spring in Fig. 8(b) occurs over more than 100 ms. The fish first pushes into the prey, applying an initial compressive force prior to performing the head flick. This is unlike SunBot, which starts the head flick from static conditions. Note that the prey in (a) tears while the "prey" in (b) does not, i.e. the spring stays attached. This tearing in (a) may explain why the real butterflyfish has a head deflection close to 30°, whereas SunBot's head only rotates around 10° at peak pull.

SunBot is inspired by the Sunburst butterflyfish but there are many key differences. The mass of a butterflyfish ranges from 20-80 g, while SunBot is 400 g. The standard length of *C. kleinii*, defined from the anterior tip of the head to the base of the soft caudal fin, can reach up to 15 cm and the specimen here is 7 cm. In contrast, SunBot is 21.5 cm in standard length. It is therefore expected that force scale and timing would vary between the animal and robot.

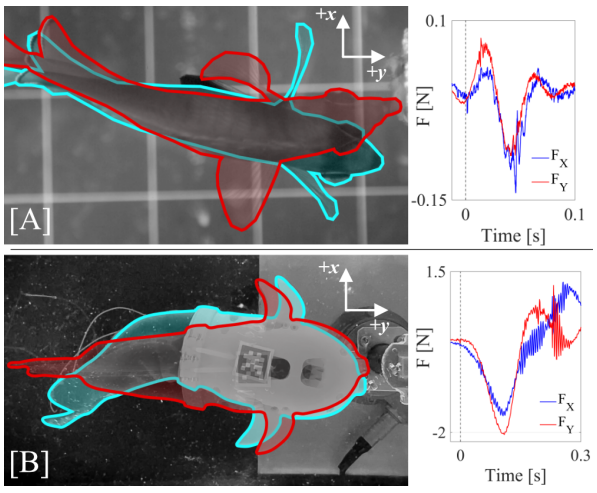

Fig. 8. (a) A sunburst butterflyfish bites at fixed prey, demonstrating lateral head motion, or head flick. (b) Sunbot pulls as a mock prey using tail-driven head flick. Both (a) and (b) show a peak in pulling forces in the negative F_x and F_y directions. In the images, the red outline indicates the initial configuration while the cyan outline represents maximum head motion.

V. Discussion

These results show the possibility of utilizing a fish-inspired robot with a single tail actuator to apply tugging forces to fixed prey. While a faster robot tail produces larger tugging forces, there are diminishing returns when it comes to increasing tail range of motion. The dynamics simulation in this work demonstrates that inertial effects play a substantial role in the application of force at the scales tested. However, modeling of fluid forces on the fish body – such as with the Large-amplitude elongated-body theory of fish locomotion [29] – should be incorporated in order to evaluate the role of water and not just inertia. More complex interactions between body shape and mechanics could also be studied with Computational Fluid Dynamics (CFD).

We acknowledge that the current state of this robotic fish is too different from its natural counterpart to draw conclusions about animal behavior from this study. SunBot is not meant to serve as a realistic model for the animal but rather to explore a new robotic function. For example, butterflyfish employ other propulsors and body mobility not possessed by SunBot, such as pectoral fins, that may contribute to tearing fixed prey. Despite differences, SunBot successfully demonstrates that it can perform lateral head motions, as inspired by observed behaviors of *C. kleinii*. This work also motivates future efforts to investigate the role of different morphological features on fish dexterity through parametric study with more biomimetic robophysical models, as well as additional study on real fish behaviors.

VI. Demonstrations

A. Tearing demonstration

In the above experiments, Sunbot's anterior point was connected to a spring and never broke free. Thus, we performed further testing to demonstrate the capability of the tail-driven head flick to achieve successful tearing manipulation. We use a nearly identical laboratory setup as mentioned in Section III. However, a new "fixed prey" is created consisting of a stack of laser cut paper strips with a 3.5 mm hole for mounting at either end. The center-to-center length of each paper strip is 25 mm and the width of the sample at its midpoint is 3.2 mm. The anterior tip of SunBot and the end mount of the force-measurement device are modified, replacing the spherical neodymium magnet attachment points for the paper. The prepared tearing demonstration setup is shown in Fig. 9. To achieve the best performance, SunBot was commanded to bend to a tail angle of 72° at the maximum possible servomotor speed.

The tearing capabilities were assessed by three separate trials, with 10-layer, 12-layer, and 18-layer paper samples.

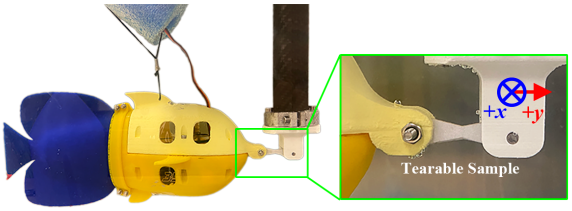

Fig. 9. SunBot affixed to force-measurement apparatus with tearable paper-based prey. A close-up photo, taken of the same posture, is highlighted on the right. The modified end mount has a slot in which the 12 stacked strips of paper can be inserted; a friction fit dowel pin then holds them in place. A machine screw attaches the other end to a similar slot on SunBot.

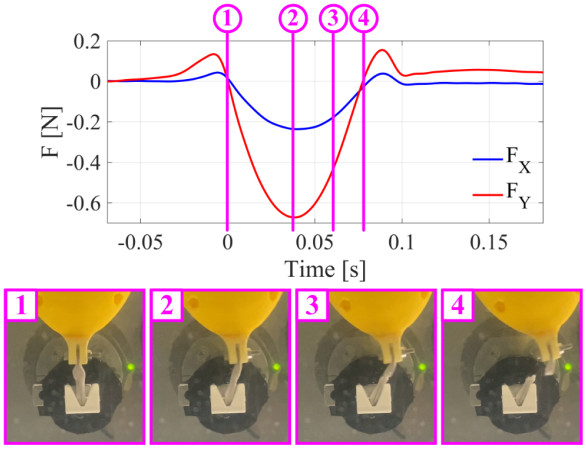

Fig. 10. Time series data of lateral force (F_x) and axial force (F_y) applied by SunBot while bending its tail in order to tear a 12-layer stacked paper substrate. Key times such as the start of the body bend (1), the peak pulling force (2), start of material failure (3), and completion of tearing (4) are labeled and their corresponding video frames are shown below.

SunBot successfully tore the 10- and 12-layer samples in a single bending motion. However, for the 18-layer sample, the robot could only partially tear the sample in one pull. In this case, we commanded SunBot to perform the same bending maneuver immediately after the failed tear. This secondary pull successfully tore the sample.

Force data was measured and synchronized to video data for the trial when tearing the 12-layer paper, presented in both Fig. 10 and Fig. 1. For this single trial, we measured a peak axial pulling force (F_y) of 0.67 N and peak lateral (F_x) pulling force of 0.24 N. Referenced from the initiation of SunBot's tail-driven head flick, the time to peak force is 50 ms and the time to failure of the prey is 60 ms.

B. Swimming demonstration

To demonstrate that SunBot is not overspecialized for tearing manipulations we tested its swimming ability in a pool. It was still tethered for data and power connections. The robot was commanded using an open-loop trajectory to bend its tail back and forth between angles of $\pm 55°$ at a frequency of 2 Hz. As shown in Fig. 11, it was able to swim at a speed of approximately 0.6 body lengths (BL) per second, or a forward velocity of 0.15 m/s. The Strouhal number is 2.4, which is an order of magnitude larger than the range of 0.2-0.4 for biological swimmers and fliers [30]. This

Fig. 11. Overlayed video frames of SunBot swimming in an outdoor pool. The robot is able to reach speeds of up to 0.6 body lengths per second by periodic bending of the tail at 2 Hz with an amplitude of $\pm 55°$

indicates that SunBot is not a particularly efficient swimmer. As this was not a focus of the current work, future versions of SunBot could be better optimized for swimming ability.

VII. Conclusion

We present the development of a bio-inspired underwater robotic platform capable of tail-driven manipulation. Through laboratory experiments, we demonstrate that this "head flick" behavior has functionality in both controllable force application as well as tearing of substrates. The dynamics of the actuation are subsequently captured by a simulated rigid-body model. While the model lacks a consideration of fluid dynamics effects and tail deformation, the peak forces predicted by it align with observed trends in experimental results. Thus, for the conditions tested, it appears that inertial effects play a substantial role. Importantly, SunBot is not only capable of these floating manipulation tasks, but also demonstrates proficient swimming locomotion. Thus, our robotic platform motivates the use of existing open-water swimmers for new manipulation functions.

A. Future work

There are promising future pathways to expand the capabilities of the SunBot platform. Integration of a jaw or gripping mechanism would allow for repeated engagement and disengagement with different prey. The addition of more propulsors, like pectoral fins, along with increased control intelligence and perception, would allow for more advanced maneuvers. In modelling, the addition of drag forces or the implementation of more sophisticated computational fluid dynamics simulations could better inform the underlying "head flick" mechanism across an expanded range of parameters. We are also interested in better understanding the tearing mechanics of underwater prey, in order to guide future designs for real-world tasks. The ultimate goal of this work is to inform a robotic fish system capable of autonomous swimming and sampling in the field.

Acknowledgment

This work was funded by a CITRIS & Banatao Institute Seed Grant (Principal Investigator H. Stuart, co-PI P. Wainwright). J. Romero is a National Science Foundation Graduate Research Fellow (NSF GRFP #2020306552). M. Li is supported by the National Aeronautics and Space Administration through a Space Technology Research Fellowship (NSTRF #80NSSC20K1166).

REFERENCES

[1] F. Negrello, H. S. Stuart, and M. G. Catalano, "Hands in the real world," *Frontiers in Robotics and AI*, vol. 6, p. 147, 2020.

[2] A. Mazzeo, J. Aguzzi, M. Calisti, S. Canese, F. Vecchi, S. Stefanni, and M. Controzzi, "Marine Robotics for Deep-Sea Specimen Collection: A Systematic Review of Underwater Grippers," *Sensors*, vol. 22, no. 2, 2022.

[3] T. D. Eddy, V. W. Lam, G. Reygondeau, A. M. Cisneros-Montemayor, K. Greer, M. L. D. Palomares, J. F. Bruno, Y. Ota, and W. W. Cheung, "Global decline in capacity of coral reefs to provide ecosystem services," *One Earth*, vol. 4, no. 9, pp. 1278–1285, 2021.

[4] O. Khatib, X. Yeh, G. Brantner, B. Soe, B. Kim, S. Ganguly, H. Stuart, S. Wang, M. Cutkosky, A. Edsinger *et al.*, "Ocean one: A robotic avatar for oceanic discovery," *IEEE Robotics & Automation Magazine*, vol. 23, no. 4, pp. 20–29, 2016.

[5] B. H. Robison, K. R. Reisenbichler, and R. E. Sherlock, "The coevolution of midwater research and ROV technology at MBARI," *Oceanography*, vol. 30, no. 4, pp. 26–37, 2017.

[6] R. Bogue, "Underwater robots: a review of technologies and applications," *Industrial Robot: An International Journal*, vol. 42, no. 3, pp. 186–191, 2015.

[7] J. Koch and J. Leichty, "Development of a Robotic Arm for Mini-Class ROV Dexterous Manipulation," in *OCEANS 2019 MTS/IEEE SEATTLE*, 2019, pp. 1–5.

[8] N. R. Sinatra, C. B. Teeple, D. M. Vogt, K. K. Parker, D. F. Gruber, and R. J. Wood, "Ultragentle manipulation of delicate structures using a soft robotic gripper," *Science Robotics*, vol. 4, no. 33, p. eaax5425, 2019.

[9] R. K. Katzschmann, J. DelPreto, R. MacCurdy, and D. Rus, "Exploration of underwater life with an acoustically controlled soft robotic fish," *Science Robotics*, vol. 3, no. 16, p. eaar3449, 2018.

[10] J. Yu, M. Tan, S. Wang, and E. Chen, "Development of a biomimetic robotic fish and its control algorithm," *IEEE Transactions on Systems, Man, and Cybernetics, Part B (Cybernetics)*, vol. 34, no. 4, pp. 1798–1810, 2004.

[11] S. Liu, Y. Wang, Z. Li, M. Jin, L. Ren, and C. Liu, "A fluid-driven soft robotic fish inspired by fish muscle architecture," *Bioinspiration & Biomimetics*, vol. 17, no. 2, p. 026009, feb 2022.

[12] X. Tan, D. Kim, N. Usher, D. Laboy, J. Jackson, A. Kapetanovic, J. Rapai, B. Sabadus, and X. Zhou, "An Autonomous Robotic Fish for Mobile Sensing," in *2006 IEEE/RSJ International Conference on Intelligent Robots and Systems*, 2006, pp. 5424–5429.

[13] R. Mason and J. Burdick, "Experiments in carangiform robotic fish locomotion," in *Proceedings 2000 ICRA. Millennium Conference. IEEE International Conference on Robotics and Automation. Symposia Proceedings (Cat. No.00CH37065)*, vol. 1, 2000, pp. 428–435 vol.1.

[14] J. Liang, T. Wang, and L. Wen, "Development of a two-joint robotic fish for real-world exploration," *Journal of Field Robotics*, vol. 28, no. 1, pp. 70–79, 2011.

[15] Y. Zhong, Z. Li, and R. Du, "A Novel Robot Fish With Wire-Driven Active Body and Compliant Tail," *IEEE/ASME Transactions on Mechatronics*, vol. 22, no. 4, pp. 1633–1643, 2017.

[16] D. R. Bellwood and J. H. Choat, "A functional analysis of grazing in parrotfishes (family Scaridae): the ecological implications," in *Alternative life-history styles of fishes*. Springer, 1990, pp. 189–214.

[17] P. J. Motta, "Functional morphology of the feeding apparatus of ten species of Pacific butterflyfishes (Perciformes, Chaetodontidae): an ecomorphological approach," *Environmental Biology of Fishes*, vol. 22, no. 1, pp. 39–67, 1988.

[18] N. Konow and D. R. Bellwood, "Prey-capture in Pomacanthus semicirculatus (Teleostei, Pomacanthidae): functional implications of intramandibular joints in marine angelfishes," *Journal of Experimental Biology*, vol. 208, no. 8, pp. 1421–1433, 2005.

[19] J. M. Copus and A. C. Gibb, "A forceful upper jaw facilitates picking-based prey capture: biomechanics of feeding in a butterflyfish, Chaetodon trichrous," *Zoology*, vol. 116, no. 6, pp. 336–347, 2013.

[20] T. Perevolotsky, C. H. Martin, A. Rivlin, and R. Holzman, "Work that body: fin and body movements determine herbivore feeding performance within the natural reef environment," *Proceedings of the Royal Society B*, vol. 287, no. 1938, p. 20201903, 2020.

[21] C. M. Martinez, A. J. Tovar, and P. C. Wainwright, "A novel intramandibular joint facilitates feeding versatility in the sixbar distichodus," *Journal of Experimental Biology*, 2022.

[22] K. Yoshida, "Space robotics research activity with Experimental Free-Floating Robot Satellite (EFFORTS) simulators," in *Experimental Robotics III*, T. Yoshikawa and F. Miyazaki, Eds. Berlin, Heidelberg: Springer Berlin Heidelberg, 1994, pp. 561–578.

[23] X. Meng, Y. He, and J. Han, "Hybrid Force/Motion Control and Implementation of an Aerial Manipulator towards Sustained Contact Operations," in *2019 IEEE/RSJ International Conference on Intelligent Robots and Systems (IROS)*, 2019, pp. 3678–3683.

[24] E. Simetti, G. Casalino, S. Torelli, A. Sperindé, and A. Turetta, "Floating Underwater Manipulation: Developed Control Methodology and Experimental Validation within the TRIDENT Project," *Journal of Field Robotics*, vol. 31, no. 3, pp. 364–385, 2014.

[25] M. S. Li, R. van der Zande, A. Hernández-Agreda, P. Bongaerts, and H. S. Stuart, "Gripper Design with Rotation-Constrained Teeth for Mobile Manipulation of Hard, Plating Corals with Human-Portable ROVs," in *OCEANS 2019 - Marseille*, 2019, pp. 1–6.

[26] K. C. Galloway, K. P. Becker, B. Phillips, J. Kirby, S. Licht, D. Tchernov, R. J. Wood, and D. F. Gruber, "Soft Robotic Grippers for Biological Sampling on Deep Reefs," *Soft Robotics*, vol. 3, no. 1, pp. 23–33, 2016.

[27] P. Duraisamy, R. Kumar Sidharthan, and M. Nagarajan Santhanakrishnan, "Design, Modeling, and Control of Biomimetic Fish Robot: A Review," *Journal of Bionic Engineering*, vol. 16, no. 6, pp. 967–993, 2019.

[28] S. C. van den Berg, R. B. Scharff, Z. Rusák, and J. Wu, "Openfish: Biomimetic design of a soft robotic fish for high speed locomotion," *HardwareX*, vol. 12, p. e00320, 2022.

[29] M. J. Lighthill, "Large-amplitude elongated-body theory of fish locomotion," *Proceedings of the Royal Society of London. Series B. Biological Sciences*, vol. 179, no. 1055, pp. 125–138, 1971.

[30] G. K. Taylor, R. L. Nudds, and A. L. Thomas, "Flying and swimming animals cruise at a Strouhal number tuned for high power efficiency," *Nature*, vol. 425, no. 6959, pp. 707–711, 2003.